energies

MDPI

Article

Separation of ^{3}He Isotope from Liquid Helium with the Use of Entropy Filter Composed of Carbon Nanotubes

Jakub Niechciał [1,*], Wojciech Kempiński [1,*], Leszek Stobiński [2,3], Zbigniew Trybuła [1], Piotr Banat [1], Maciej Chorowski [4], Jarosław Poliński [4], Katarzyna Chołast [5] and Andrzej Kociemba [5]

1 Institute of Molecular Physics, Polish Academy of Sciences, 60-179 Poznań, Poland; trybula@ifmpan.poznan.pl (Z.T.); banat@ifmpan.poznan.pl (P.B.)
2 Faculty of Chemical and Process Engineering, Warsaw University of Technology, 00-645 Warszawa, Poland; lstob50@hotmail.com
3 Nanomaterials, Leszek Stobinski, 03-337 Warsaw, Poland
4 Department of Cryogenics and Aerospace Engineering, Wroclaw University of Science and Technology, 50-370 Wrocław, Poland; maciej.chorowski@pwr.edu.pl (M.C.); jaroslaw.polinski@pwr.edu.pl (J.P.)
5 Polish Oil and Gas Company—Odolanów, 63-430 Odolanów, Poland; katarzyna.cholast@pgnig.pl (K.C.); andrzej.kociemba@pgnig.pl (A.K.)
* Correspondence: jakub.niechcial@ifmpan.poznan.pl (J.N.); wojkem@ifmpan.poznan.pl (W.K.)

Abstract: The ^{3}He isotope finds applications in many areas of science and industry, the most important of which are cryogenics, where ^{3}He allows for achieving millikelvins in dilution refrigerators, and public security with ^{3}He detectors of radioactive materials at airports and important buildings. ^{3}He is also used in medicine for lung tomography. One of the most extraordinary future applications is the use of ^{3}He in fusion reactors for clean energy. ^{3}He is currently very expensive, with prices reaching USD 2750 for 1 liter of gas in normal conditions; thus, more effort is put into finding economically viable methods to acquire this isotope. The article shows research results of acquiring the ^{3}He isotope from liquid helium by a quantum separation method with the use of entropy filters based on new carbon nanomaterials: purified multiwall carbon nanotubes (MWCNTs) and purified multiwall carbon nanotubes decorated with ZrO_2 nanoparticles. MWCNTs were bundled and applied in the form of pressed tablets with fixed sizes. The research was conducted at the low-temperature region, where helium exhibits its quantum properties by undergoing a phase transition to the superfluid phase at the *lambda* temperature: $T_\lambda = 2.18$ K. Entropy filters work below this temperature.

Keywords: entropy filter; carbon nanotubes; quantum filtration; isotope separation; ^{3}He isotope

check for updates

Citation: Niechciał, J.; Kempiński, W.; Stobiński, L.; Trybuła, Z.; Banat, P.; Chorowski, M.; Poliński, J.; Chołast, K.; Kociemba, A. Separation of ^{3}He Isotope from Liquid Helium with the Use of Entropy Filter Composed of Carbon Nanotubes. *Energies* **2021**, *14*, 6832. https://doi.org/10.3390/en14206832

Academic Editor: Muhammad Aziz

Received: 5 August 2021
Accepted: 15 October 2021
Published: 19 October 2021

Publisher's Note: MDPI stays neutral with regard to jurisdictional claims in published maps and institutional affiliations.

Copyright: © 2021 by the authors. Licensee MDPI, Basel, Switzerland. This article is an open access article distributed under the terms and conditions of the Creative Commons Attribution (CC BY) license (https://creativecommons.org/licenses/by/4.0/).

1. Introduction

From the end of the 1960s, the annual global energy consumption increased almost 3.5 times [1], leading us to look for sources that both supply stable and safe energy production, and are also in line with the sustainable development of the global economy. EU restrictions on traditional energy sources based on Earth gas and coal enforce solutions that satisfy both the economical calculation and pro-ecological regulations [2]. One of the solutions that could fulfill these requirements is fusion power, where ^{3}He is expected to be useful as a fusion fuel [3,4]. Thus, it is of utmost importance to obtain this isotope as effectively and economically as possible. The development of an industrial method for the separation of ^{3}He and ^{4}He isotopes in liquid helium (LHe) was mentioned in a U.S. Congress report as an important method from the viewpoint of energetics based on the production of clean energy [5,6]. Methods for the separation of ^{3}He-^{4}He mixture have been used for a long time [7–9], but the most interesting are those conducted at low temperatures [10–12], utilizing quantum effects occurring in superfluid helium that allow for the use of entropy filters composed of various materials [13,14]. In our case, these are modern carbon nanomaterials: pure and ZrO_2-decorated bundled multiwalled carbon nanotubes (MWCNTs) in the form of pressed tablets of a certain size.

2. State of Research on Entropy Filters

Decreasing temperature to the lambda temperature T_λ = 2.18 K and below allows us to generate a spectacular quantum state in liquid ^{4}He [10,11] known as the Bose-Einstein condensate. It is a dramatic change in the physical properties of helium, thus qualifying it as a superfluid state. This phase transition was named lambda transition due to the characteristic shape of specific heat vs temperature dependence (resembling the Greek letter λ). Helium below T_λ, also named He II, can be considered as a mixture of normal and superfluid phases, described with the phenomenological Tisza model:

$$\rho = \rho_n + \rho_s \tag{1}$$

where:
ρ—density of He II;
ρ_n—density of the normal component;
ρ_s—density of the superfluid component.

The concentration of normal and superfluid components in the mixture is a function of temperature. The superfluid component appears at T_λ, and its share increases with decreasing temperature, whereas the normal component decreases:

$$\frac{\rho_n}{\rho} = \left(\frac{T}{T_\lambda}\right)^{5.6} \tag{2}$$

where:
ρ_n—density of the normal component of He II;
ρ—total helium density;
T_λ—temperature of the lambda point (2.18 K);
T—temperature.

The peculiarity of this phase is the lack of viscosity. For the extraction of ^{3}He, it is necessary to disturb the equilibrium by locally delivering energy to increase the temperature, which in turn increases the ρ_n/ρ ratio (and decreases the ρ_s/ρ ratio). The whole system attempts to recover concentration balance, so the superfluid component flows into the area with increased temperature, while the normal one flows out. The application of an entropy filter would allow for separating these flows, as the superfluid component can flow through the filter, while the normal one is stopped due to having nonzero viscosity.

^{3}He atoms are fermions, do not become superfluid at T_λ, and are in a normal state down to 0.3 mK, where the pairing of ^{3}He atoms creates bosons that can condensate. Thus, in the temperature region of 0.003–2.18 K, ^{3}He cannot flow through the entropy filter. The separation system used in this research works as a thermomechanical pump and utilizes the "fountain effect" described by London's equation [15].

$$\Delta p = \rho \cdot s \cdot \Delta T \tag{3}$$

where:
Δp—pressure difference;
ρ—density;
s—entropy;
ΔT—temperature difference.

The fountain effect allows for the removal of superfluid ^{4}He from the ^{3}He-^{4}He mixture, thus enriching the mixture in the ^{3}He isotope [11]. The lower the working temperature is, the higher the amount of ^{4}He atoms that can make their way through the entropy filter, and the higher the flow capacity of the filter. This capacity also depends on the materials used to construct the filter.

In gas and liquid separation, various materials are used. Recently, graphene became very popular in molecular and atomic separation processes [16]. For example, at temperatures higher than 200 K, gaseous ^{4}He penetration through graphene membrane is much higher than that for other gases [7]. These results show that graphene separators are more effective than traditional polymer membranes are. Nitrogen-doped graphene membranes were used to separate ^{3}He and ^{4}He via a quantum tunneling effect, but the effectiveness of this process was relatively low [9].

Entropy filters working below T_λ are composed of porous materials or form a porous texture with a developed network of canals for the percolation of the ^{4}He superfluid component, but stopping the normal component, including ^{3}He. These can also be braided fibers [17]. Table 1 shows the materials used for the construction of entropy filters.

Table 1. Entrophy filters.

Research Team	Entrophy Filters	Length	Pore Diameter
S. Hamaguchi [14]	Al_2O_3	2–10 mm	1–2 μm
S. Hamaguchi [14]	CSi	1.2–1.5 mm	10.8–20 μm
H. Nakai [13]	Al_2O_3	5–10 mm	0.4–1 μm
B. Maekawa [18]	Al_2O_3	2–4 mm	2 μm
B. Baudouy [19]	Al_2O_3	2–4 mm	2 μm
B. Baudouy [19]	CSi	1.2–1.5 mm	10.8–20 μm
M.C. Dalban [17]	MIWF †	3.08 mm	no data
H. Allain [20]	membrane	1.5 mm	10.8 μm

† Multilayered impregnated woven-fiber 20-layer preimpregnated insulation.

The materials in Table 1 had pores of the size of several μm. The nanomaterials in our research had percolation canals in the order of nano- and micrometers. Materials were chosen for this research to ensure that the required conditions are fulfilled [10]. Porous materials used in our work can be divided into two categories: pure and decorated with chosen nanoparticles. In our case, the latter was composed of ZrO_2, and their role was to keep a certain distance between MWCNTs in the process of pressing them into a tablet.

3. As-prepared Carbon Nanotubes and Purified Decorated MWCNTs

Nanomaterials LS Co. (Warsaw, Poland) deposited ZrO_2 nanoparticles on the surface of bundled purified MWCNTs [21]. Scanning electron microscopy images of these materials are shown in Figure 1: (a) purified MWCNTs and (b) purified MWCNTs decorated with ZrO_2 nanoparticles, both before the process of pressing into tablets.

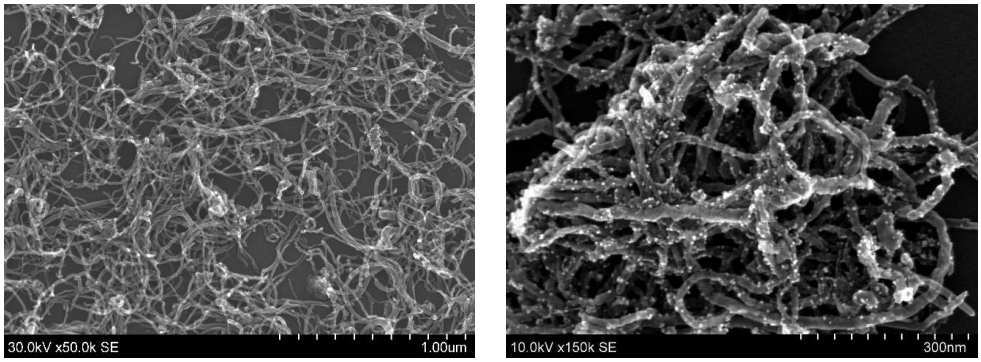

(**a**) (**b**)

Figure 1. Images of MWCNTs before making tablets: (**a**) purified bundled MWCNTs; (**b**) purified bundled MWCNTs decorated with ZrO_2 nanoparticles, which are visible as light spots on the nanotube surface. Courtesy of Nanomaterials LS.

MWCNTs used in our studies were produced by CNT Co., Ltd. (Korea, product number: CTUBE100). Nanotube diameters were in the range of 20–40 nm. Impurities visible at SEM images were mainly amorphous carbon and Fe–C particles. As-prepared MWCNTs contained more than 90% weight of carbon nanotubes. Other impurities (amorphous carbon and catalyst nanoparticles) were removed after a 6 h process of etching with 65% nitric acid at 120 °C. After this reaction, oxidized MWCNTs were successively eluted with deionised water, then with 5% of ammonia water, and then with deionised water until the pH of the filtrate was stabilized. During the oxidation process, multiwall carbon nanotubes were functionalized with different kinds of oxygen groups, such as -OH, C-O-C, C=O, and –COOH [21]. In the presence of ammonia water, –COOH groups were converted into ammonium carboxylate groups $–COONH_4$. These groups could easily dissociate in the water environment into $–COO^-$ anions and NH^+ cations. The specific surface of the as-prepared MWCNTs was approx. 180 m^2/g; after the oxidation process, it was approx. 260 m^2/g. The water suspension with oxidized MWCNTs (1 wt%) was sonicated around 30 min, and the water solution of $ZrOCl_2$ was added (SIGMA-Aldrich). After 15 min of solution sonication, 1 M NaOH solution was added until it had reached pH 10–11. After 15 min of stirring, the resulting suspension was placed into a pressure microwave reactor.

The reaction mixture was maintained at 250 °C and 55 bar for 20 minutes. After this process, the suspension was filtrated, and the deposited ZrO_2/MWCNTs composite was rinsed several times with distilled water and twice with ethanol. Then, it was dried for 12 h at 80 °C. The size of ZrO_2 nanoparticles obtained by the above-mentioned hydrothermal method was in the 5–10 nm range. Depending on initial concentrations of $ZrOCl_2$ and MWCNTs-COOH, the yield of ZrO_2 nanoparticle deposition on the MWCNT surface varied from 0.01 up to 99.5 wt %. In our helium filtration experiments, we used a nanocomposite with the following composition: 20 wt % ZrO_2 and 80 wt % MWCNTs. Depending on the desired size of the final tablet, 10–100 g of dry powder of ZrO_2/MWCNTs composite was placed inside a steel pressure matrix and tamped with a steel plunger. Then, the powder was pressed with pressure power of 4.5 to 7.5 kbar for 15 min. After that, the steel plunger was slowly released until pressure was almost equal to the atmospheric one. Examples of the obtained tablets are shown in Figure 2. Tablets with diameters of 1–2.5 cm and height of 1–4 cm were obtained.

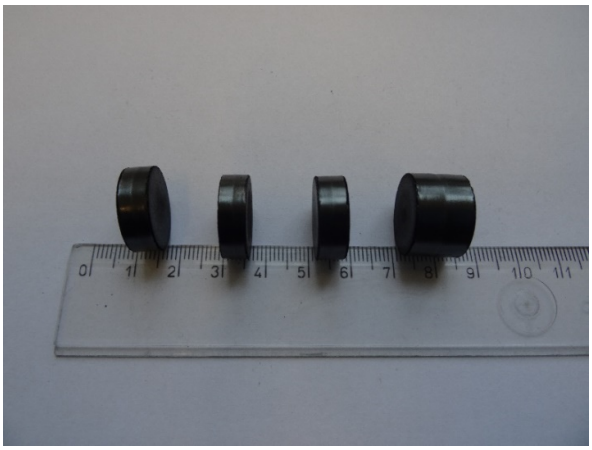

Figure 2. Pressed tablets made of ZrO_2/MWCNTs—ZrO_2 (20 wt.%)/MWCNTs (80 wt.%) (Courtesy of Nanomaterials LS).

4. Measurement Stations

Research on entropy filters focused on two basic parameters related to the separation of helium isotopes: flow capacity (fountain effect) and filter effectiveness (the highest possible for given experimental parameters level of ^3He concentration).

A special experimental setup was used for determining filter capacity—see Figure 3.

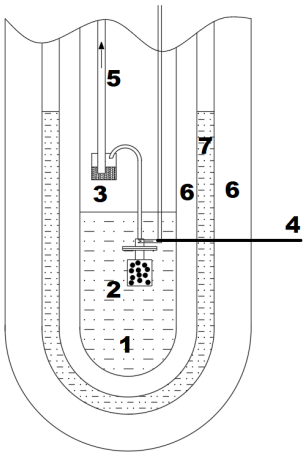

Figure 3. Experimental setup for determining the filter capacity: 1—mixture ^{3}He-^{4}He, 2—entropy filter, 3—vessel for ^{4}He, 4—heater, 5—recovery of ^{4}He, 6—vacuum, 7—vessel of liquid nitrogen.

The key elements of this apparatus were: entropy filter (2), heater (4), and a vessel above them (3). The principle of operation of this system was to run the fountain effect so that the helium with lowered concentration of ^{3}He was collected behind the entropy filter in a vessel (3). The rate of filling of the vessel from the start up of the fountain effect is a measure of flow capacity of the examined entropy filter.

The maximal mass of the liquid helium that could be filtrated was 2.5 kg. Filter effectiveness was tested with the setup presented in Figure 4.

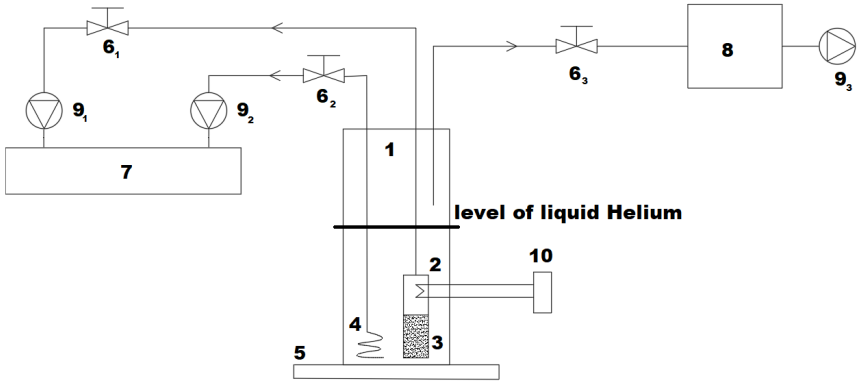

Figure 4. Test stand for determining the effectiveness of examined process: 1—helium container 25 LHe, 2—heater, 3—entropy filter, 4—capillary with heat exchanger, 5—scales, $6_{1,2,3}$—valves, 7—recovery of helium, 8—mass spectrometer, $9_{1,2,3}$—pumps, 10—power supply

The main elements of the station were:
1—helium container with filtering setup (25 liters of LHe);
2—heater for running of the thermomechanical pump—the fountain effect;
3—entropy filter (ZrO_2(20 wt.%)/MWCNTs(80 wt %));
4—heat exchanger ending with a capillary for cooling helium with simultaneous reduction in the ^{3}He losses (see [10] for more details);
5—scales for measuring helium mass changes during the experiment;
6—regulating valves;
7—recovery system of helium;
8—mass spectrometer for determination of the concentration of ^{3}He in liquid ^{3}He-^{4}He mixture in the container (1);
9—pumps;
10—power supply for heater.

Heat exchanger (4), described in [10], enabled the cooling of helium down to 1.8 K. The resistive element (heater) was supplied with power no larger than enough to ensure the laminar flow of superfluid component (compare with Figure 6). The cooling procedure of the system is schematically presented in Figure 5, and the most important temperature ranges are marked.

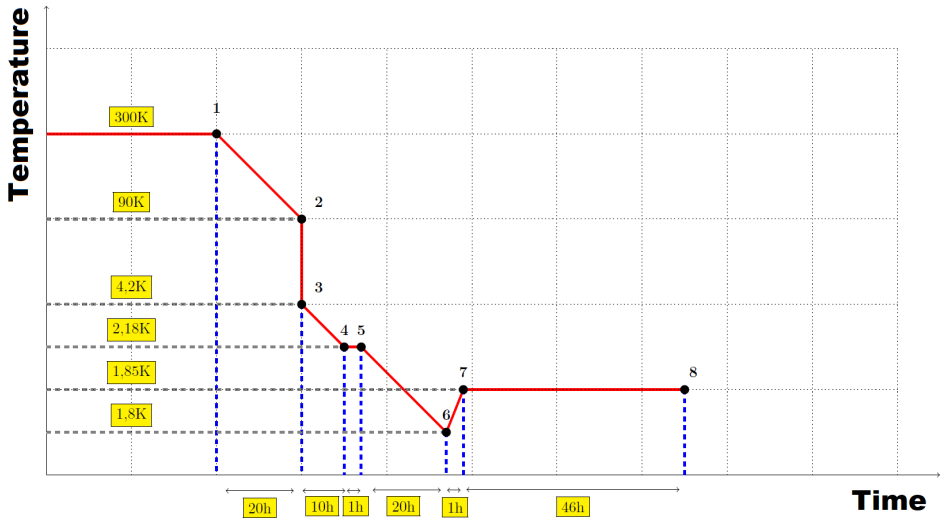

Figure 5. Schematic presentation of cooling process: 1–2, helium container cooling; 2–3, liquid helium overflow; 3–4, cooling to T_λ; 4–5, lambda front [10]; 5–6, cooling of the system to the filtration temperature of 1.8 K; 6–8, quantum filtration via the fountain effect.

Ranges are characterized as follows:
1–2, cooling of the helium container (1) from approx. 300 to 90 K by thermal shield cooled with LN_2 with helium atmosphere inside the container for the whole time;
2–3, filling container (1) with 25 liters of LHe with simultaneous cooling to 4.2 K;
3–4, start up of the heat exchanger, and obtaining T_λ (2.18 K);
4–5, lambda front movement (see [10]);
5–6, cooling down to the working range of entropy filter (1.8–1.9 K);
6–8, quantum filtration via fountain effect.

5. Results and Discussion

Entropy filters were examined for the capacity of the superfluid component flow and for the effectiveness of the ^{3}He isotope separation (observed as the increase of ^{3}He/^{4}He ratio in the normal component of ^{3}He-^{4}He mixture). Measurements of the flow capacity were performed with the experimental setup schematically presented in Figure 3. Figure 6 shows the comparison of the obtained results for purified MWCNTs and ZrO_2/MWCNTs composites with the averaged results from research by H. Nakai team [13] obtained at 1.8 K for the standard entropy filters made of Al_2O_3 powders with varying grain size. Graph shows that the slope of the curve versus the power axis for the obtained series for MWCNTs was larger than that for Al_2O_3. This means a higher flow capacity of both types of MWCNTs filters.

Setup for the measurements of capacity of entropy filters was prepared for the filtration process working with a certain amount of helium. Due to this, the enrichment of the LHe mixture in ^{3}He was possible only to a limited extent—approximately 2.3 kg of helium could be filtered (which translates to 20 liters of LHe). This particular experimental setup was already described in detail in our previous paper [10].

The measurements of separation effectiveness were performed on the sample of ZrO_2/MWCNTs. This was chosen after the comparison of the filter flow capacity test results for an entropy filter composed of purified MWCNTs and the one composed of ZrO_2/MWCNTs composite—see Figure 6. Analysis of the regression lines showed that the

line for the latter sample starts almost exactly at zero. This means that thermomechanical pump works even for the lowest applied power. This allows for the smooth (not jumpy) regulation of flow until reaching the final parameters of the filtration process — during the experiment, it was crucial to precisely control the pressure downstream of the entropy filter.

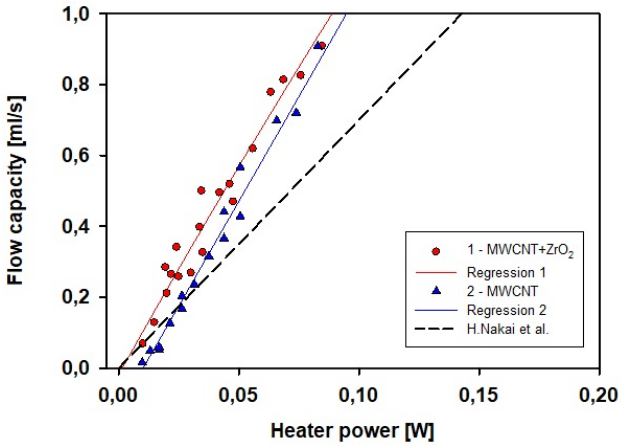

Figure 6. Filter flow capacity comparison with Nakai's team results [13].

Two series with different levels of thermal excitation of the fountain effect were registered. Results are presented in Figures 7 and 8. Concentration measurement was performed on a QMS700 spectrometer. Exemplary results of the ^{3}He concentration measurement at the beginning and in the intermediate stage of the filtration effectiveness are shown in Figure 7a,b. The QMS700 spectrometer allows for detection of 10^{-3} ppm of ^{3}He, but due to the relatively high background level, as shown in Figure 7, the experimental assumed error was at the level of 10^{-2} ppm (too low to mark in Figure 8).

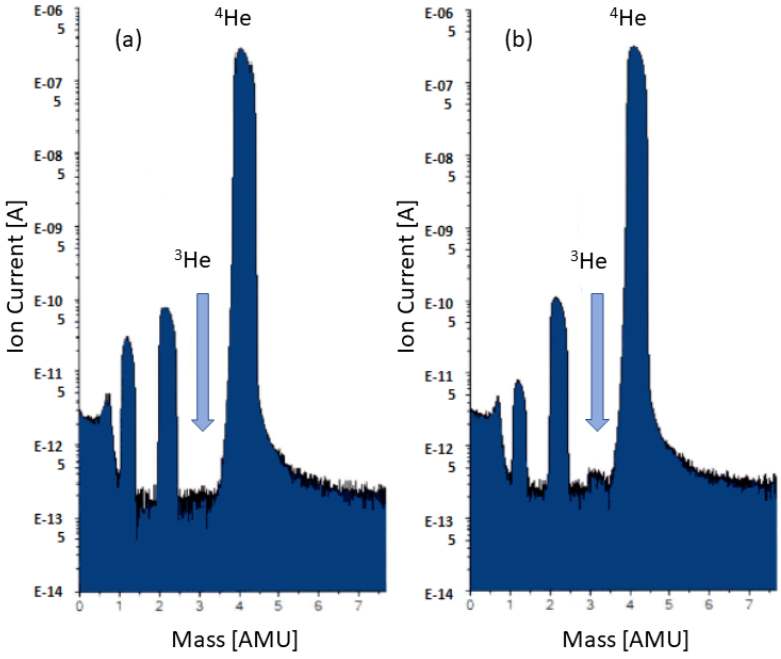

Figure 7. Results of two measurements of ^{3}He concentration: (**a**) beginning and (**b**) intermediate stage.

Figure 7 presents ^{3}He concentration measurements for two stages of the experiment: initial with ^{3}He concentration of 0.2 ppm (Figure 7a) and one of the intermediate stages of the enrichment process (Figure 7b), where ^{3}He concentration increased to 1.1 ppm. Results of two experiments showing the increase in ^{3}He concentration during the operation of entropy filter in different experimental conditions are presented in Figure 8. An experiment was conducted with heater power of 26.88 mW, and the second with 55.00 mW.

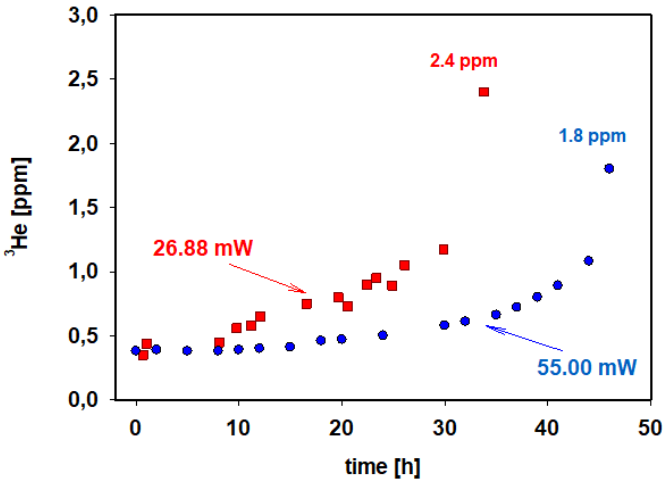

Figure 8. Concentration of ^{3}He in the ^{3}He-^{4}He mixture vs time for two filtration processes—one with heater power of 26.88 mW (red squares) and one with 55.00 mW (blue circles). Entropy filter was composed of ZrO_2/MWCNTs composite.

Initial level of ^{3}He concentration for both processes presented in Figure 8 is ≈0.4 ppm, which is higher than the one showed earlier for the unprocessed ^{3}He-^{4}He mixture (≈0.2 ppm). This is because, before starting to gather samples for mass spectrometry, ^{3}He concentration slightly increased during the process of cooling the system by the capillary, which is the part of heat exchanger (Stages 3–6 in Figure 5). Results for different power levels used, presented in Figure 8, significantly differed: the application of the lower exciting power resulted in the higher concentration obtained in a shorter time. This is the result of the apparently crucial way of the regulation and stabilization of upstream and downstream pressure in the entropy filter. The upstream filter pressure was the same as in the whole helium container containing the enriched ^{3}He-^{4}He mixture. During the experiment, this pressure was stable for the chosen temperature. Downstream filter pressure strongly depended on the flow rate of the superfluid component. Increasing the flow rate made it more difficult to maintain stable conditions downstream of the filter although, for all used power levels, the flow was still in the laminar regime (compare with Figure 6). The downstream filter pressure controls the rate of the removal of filtered ^{4}He from the system, so its increase should lead to a more effective process. However, increasing flow capacity with a higher heating level (55.00 mW case) results in a sudden uncontrollable increase in pressure downstream of the filter, which led to a excited flow and worsened the filtration conditions. Lastly, both time and concentration were better for gentler conditions.

6. Conclusions

Our method of increasing the concentration of ^{3}He in the ^{3}He-^{4}He mixture, utilizing composite entropy filters in connection with careful control of filtration process conditions, is an important point on the roadmap to the future production of significant amounts of ^{3}He, which is increasingly desirable for various purposes. This method, after improvements, could relatively easily be introduced into large installations producing LHe, which is a huge advantage over other, more exotic ways, for example, the extraction of ^{3}He from the Moon's surface.

Quantum filtration utilizing entropy filters made from carbon-based materials is especially interesting because these materials can be obtained in various forms and with strict control over their morphology [22,23], which in turn might lead to the increase in the effectiveness of described process.

The presented results in Figure 8 suggest that there is an excitation power for which the filtration process is most effective. The determination of this optimal power level is one of our future goals.

Author Contributions: Conceptualization, W.K., Z.T., M.C. and J.P.; Data curation, J.N., L.S. and P.B.; Formal analysis, W.K., M.C. and J.P.; Investigation, J.N., W.K. and Z.T.; Methodology, P.B. and M.C.; Resources, K.C. and A.K.; Software, P.B.; Supervision, W.K., Z.T., M.C., K.C. and A.K.; Validation, L.S.; Writing–original draft, J.N., W.K., L.S. and J.P. All authors have read and agreed to the published version of the manuscript.

Funding: This work was supported by the grant NCBiR INNOTECH K1/IN1/11/159127/NCBR/12, and partially by the Wroclaw Technology Park.

Conflicts of Interest: The authors declare no conflict of interest.

References

1. Looney, B. *BP Statisctical Review of World Energy*, 69th ed.; Statistical Review of World Energy BP p.l.c': London, UK, 2020. Available online: https://www.bp.com/en/global/corporate/energy-economics/statistical-review-of-world-energy.html (accessed on 18 September 2021).
2. Capros, P. *EU Reference Scenario 2016: Energy, Transport and GHG Emmision Trends to 2050*; Publications Office of the European Union: Luxembourg, 2016. [CrossRef]
3. Kukulin, V.; Voronchev, V. Pinch-Based Thermonuclear D3He Fusion Driven by a Femtosecond Laser. *Phycis At. Nucl.* **2009**, *73*, 1418–1426. [CrossRef]
4. Simko, T.; Gray, M. Lunar Helium-3 Fuel for Nuclear Fusion: Technology, Economics, and Resources. *World Futur. Rev.* **2014**, *6*, 158–171. [CrossRef]
5. Shea, D.A.; Morgan, D. *The Helium-3 Shortage: Supply, Demand, and Options for Congress*; Congressional Research Service: 2010. Available online: https://www.researchgate.net/publication/285860794_The_Helium-3_Shortage_Supply_Demand_and_Options_for_Congress (accessed on 18 September 2021).
6. Cho, A. He-3 Shortage Could Put Freeze on Low Temperature Research. *Science* **2009**, *326*, 778. [CrossRef] [PubMed]
7. Schrier, J. Helium Separation Using Porous Graphene Membranes. *J. Phys. Chem. Lett.* **2010**, *15*, 2284–2287. [CrossRef]
8. Jiang, D.; Cooper, V.; Dai, S. Porous Graphene as the Ultimate Membrane for Gas Separation. *Nano Lett.* **2009**, *9*, 4019–4024. [CrossRef] [PubMed]
9. Hauser, A.; Schwerdtfeger, P. Nanoporous Graphene Membranes for Efficient ^{3}He /^{4}He Separation. *J. Phys. Chem. Lett.* **2012**, *3*, 209–2012. [CrossRef]
10. Kempiński, W.; Łoś, S.; Trybuła, Z.; Chorowski, M.; Poliński, J.; Niechciał, J.; Jaskólski, T.; Chołast, K.; Kociemba, A. Helium3 isotope separation and lambda front observation. *Sep. Purif. Technol.* **2019**, *210*, 76–280. [CrossRef]
11. Chorowski, M.; Polinski, J.; Kempiński, W.; Trybuła, Z.; Łoś, S.; Chołast, K.; Kociemba, A. Continuous Flow System for Controlling Phases Separation Near Lambda Transition. *AIP Conf. Proc.* **2014**, *1573*, 276–284. [CrossRef]
12. Niechciał, J.; Banat, P.; Kempiński, W.; Trybuła, Z.; Chorowski, M.; Poliński, J.; Chołast, K.; Kociemba, A. Operational Costs of He3 Separation Using the Superfluidity of He4. *Energies* **2020**, *13*, 6134. [CrossRef]
13. Nakai, H.; Kimura, N.; Murakami, M.; Haruyama, T.; Yamamotoa, A. Superfluid helium flow through porous media. *Cryogenics* **1996**, *36*, 667–673. [CrossRef]
14. Hamaguchi, S.; Maekawa, R.; Okamura, T.; Baudouy, B. Experimental and Numerical Studies on Thermal Hydraulic Characteristics of He II through Porous Mediar. *AIP Conf. Proc.* **2006**, *823*, 105–112. [CrossRef]
15. London, H. Thermodynamics of the thermomechanical effect of liquid He II. *Nature* **1939**, *142*, 484–496. [CrossRef]
16. Celebi, K.; Buchheim, J.; Wyss, R.M.; Droudian, A.; Gasser, P.; Shorubalko, I.; Kye, J.; Lee, C.; Park, H. Ultimate Permeation Across Atomically Thin Porous Graphene. *Science* **2014**, *344*, 289–292. doi: 10.1126/science.1249097. [CrossRef] [PubMed]
17. Dalban-Canassy, M.; Sciver, S.V. Steady Counterflow He II Heat Transfer Through Porous Media. *AIP Conf. Proc.* **2010**, *1218*, 1327–1334. [CrossRef]
18. Maekawa, R.; Baudouy, B. Heat Transfer through Porous Media in the Counterflow Regime of He II. *AIP Conf. Proc.* **2003**, *710*, 983–990. [CrossRef]
19. Baudouy, B.; Juster, F.; Allain, H.; Prouzet, E.; Larbot, A.; Maekawa, R. Heat Transfer through Porous Media in Static Superfluid Helium. *AIP Conf. Proc.* **2006**, *823*, 1418–1426. [CrossRef]
20. Allain, H.; Baudouy, B. Investigation of Transient Heat Transfer in Porous Media in He II. *AIP Conf. Proc.* **2008**, *985*, 208–214. [CrossRef]

21. Stobinski, L.; Lesiak, B.; Kover, L.; Toth, J.; Biniak, S.; Trykowski, G.; Judek, J. Multiwall carbon nanotubes purification and oxidation by nitric acid studied bythe FTIR and electron spectroscopy methods. *J. Alloy. Compd.* **2010**, *501*, 77–84. [CrossRef]
22. Łoś, S.; Duclaux, L.; Kempiński, W.; Połomska, M. Size Effect in the Characterization of Activated Nanostructured Carbon. *Microporous Mesoporous Mater.* **2010**, *130*, 21–25. [CrossRef]
23. Kempiński, W.; Łoś, S.; Kempiński, M.; Markowski, D. Experimental techniques for the characterization of carbon nanoparticles—A brief overview. *Beilstein J. Nanotechnol.* **2014**, *5*, 1760–1766. [CrossRef] [PubMed]